

# Synchronization for OFDM-Based Systems

Yu-Ting Sun and Jia-Chin Lin  
National Central University, Taiwan,  
R.O.C

## 1. Introduction

Recently, orthogonal frequency division multiplexing (OFDM) techniques have received great interest in wireless communications for their high speed data transmission. OFDM improves robustness against narrowband interference or severely frequency-selective channel fades caused by long multipath delay spreads and impulsive noise. A single fade or interferer can cause the whole link to fail in a single carrier system. However, only a small portion of the subcarriers are damaged in a multicarrier system. In a classical frequency division multiplexing and parallel data systems, the signal frequency band is split into  $N$  nonoverlapping frequency subchannels that are each modulated with a corresponding individual symbol to eliminate interchannel interference. Nevertheless, available bandwidth utilization is too low to waste precious resources on conventional frequency division multiplexing systems. The OFDM technique with overlapping and orthogonal subchannels was proposed to increase spectrum efficiency. A high-rate serial signal stream is divided into many low-rate parallel streams; each parallel stream modulates a mutually orthogonal subchannel individually. Therefore, OFDM technologies have recently been chosen as candidates for fourth-generation (4G) mobile communications in a variety of standards, such as 802.16m and LTE/LTE-A.

## 2. OFDM fundamentals

### 2.1 System descriptions

The block diagram of an OFDM transceiver is shown in Fig. 1. Information bits are grouped and mapped using M-phase shift keying (MPSK) or quadrature amplitude modulation (QAM). Because an OFDM symbol consists of a sum of subcarriers, the  $n$ -th  $N \times 1$  mapped signal symbol  $X_n$  is fed into the modulator using the inverse fast Fourier transform (IFFT). Then, the modulated signal  $x_n$  can be written as

$$x_n = \frac{1}{N} \sum_{k=0}^{N-1} X_k e^{j2\pi kn/N}, \quad n = 0, 1, \dots, N-1 \quad (1)$$

where  $N$  is the number of subcarriers or the IFFT size,  $k$  is the subcarrier index,  $n$  is the time index, and  $1/N$  is the normalized frequency separation of the subcarriers. Note that  $x_n$  and  $X_k$  form an  $N$ -point discrete Fourier transform (DFT) pair. The relationship can be expressed as

$$X_n = \text{DFT}_N \{x_n\} = \frac{1}{N} \sum_{k=0}^{N-1} x_k e^{-j2\pi kn/N}, \quad n = 0, 1, \dots, N - 1 \quad (2)$$

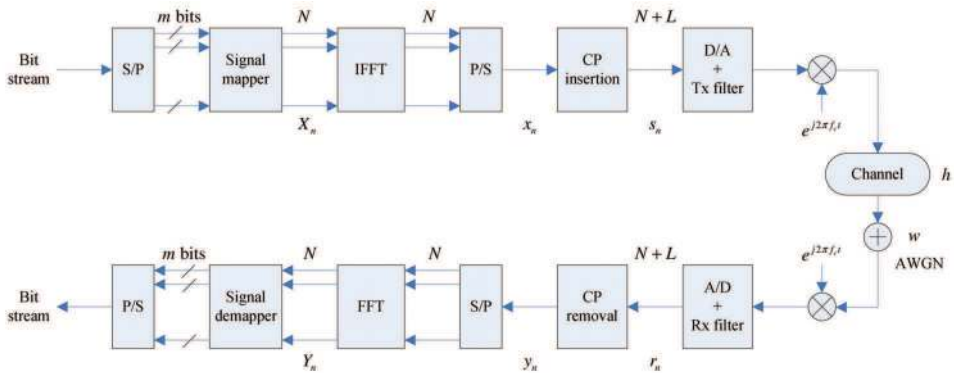


Fig. 1. The block diagram of the OFDM transceiver

The data symbol  $X_k$  can be recovered approximately by using a DFT operation at the receiver if the orthogonality of the OFDM symbol is not destroyed by intersymbol interference (ISI) and intercarrier interference (ICI). A cyclic prefix (CP) is used in an OFDM system to prevent ISI and ICI. The CP usually repeats the last  $L$  samples of an OFDM block and then is arranged in front of the block. The resulting symbol  $s_n$  can be represented as

$$s_n = \begin{cases} x_{N+n'} & n = -L, -L + 1, \dots, -1 \\ x_{n'} & n = 0, 1, \dots, N - 1 \end{cases} \quad (3)$$

The transmitted signal may pass through a channel  $h$  depending on the environments. The receiver signal  $r_n$  can be written as

$$r_n = s_n \otimes h + w \quad (4)$$

where  $w$  denotes the additive white Gaussian noise (AWGN). The data symbol  $Y_n$  can be recovered by using a DFT operation and is determined as

$$Y_n = \frac{1}{N} \sum_{k=0}^{N-1} y_k e^{j2\pi kn/N}, \quad n = 0, 1, \dots, N - 1 \quad (5)$$

Fig. 2 (a) shows the spectrum of an OFDM subchannel, and (b) shows an entire OFDM signal. At the maximum value of each subcarrier frequency, all other subcarrier spectra are null. The relationship between the OFDM block and CP is depicted clearly in Fig. 3.

The OFDM technique offers reliable effective transmission; however, it is far more vulnerable to symbol timing error and carrier frequency offset. Sensitivity to symbol timing offset is much higher in multicarrier communications than in single carrier communications because of intersymbol interference. The mismatch or instability of the local oscillator inevitably causes an offset in the carrier frequency that can cause a high bit error rate and performance degradation because of intercarrier interference. Therefore, the unknown

OFDM symbol arrival times and mismatch/instability of the oscillators in the transmitter and the receiver are two significant synchronization problems in the design of OFDM communications. A detailed description of symbol timing error and carrier frequency offset is given in the following sections.

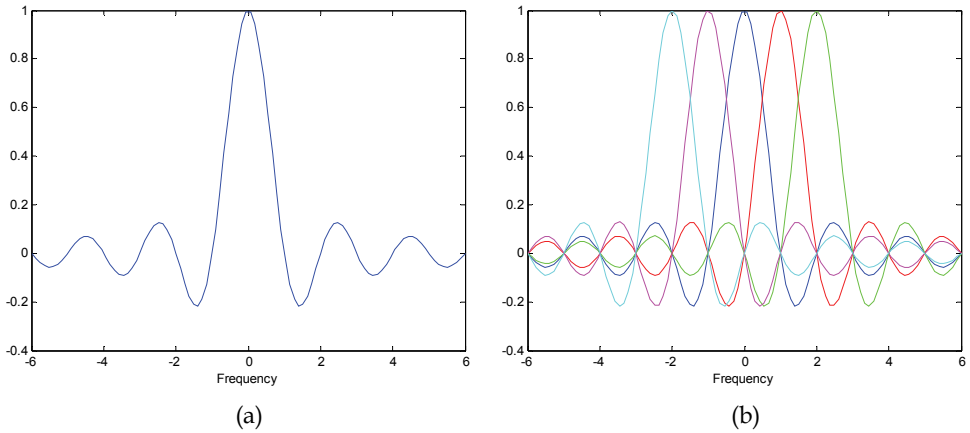


Fig. 2. Spectra of (a) an OFDM subchannel and (b) an OFDM signal

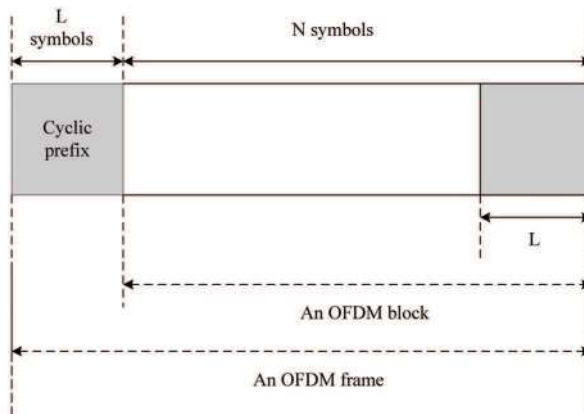


Fig. 3. An OFDM symbol with a cyclic prefix

**2.2 Synchronization issues**

**2.2.1 Timing offset**

OFDM systems exploit their unique features by using a guard interval with a cyclic prefix to eliminate intersymbol interference and intercarrier interference. In general, the symbol timing offset may vary in an interval that is equal to the guard time and does not cause intersymbol interference or intercarrier interference. OFDM systems have more robustness to compare with carrier frequency offset. However, a problem arises when the sampling

frequency does not sample an accurate position; the sensitivity to symbol timing offset increases in OFDM systems. Receivers have to be tracked time-varying symbol timing offset, which results in time-varying phase changes. Intercarrier interference comes into being another attached problem. Because an error in the sampling frequency means an error in the FFT interval duration, the sampled subcarriers are no longer mutually orthogonal. The deviation is more severe as the delay spread in multipath fading increases; then, the tolerance for the delay spread is less than the expected value. As a result, timing synchronization in OFDM systems is an important design issue to minimize the loss of robustness.

### 2.2.2 Carrier frequency offset

In section 2.1, it is evident that at all OFDM subcarriers are orthogonal to each other when they have a different integer number of cycles in the FFT interval. The number of cycles is not an integer in FFT interval when a frequency offset exists. This phenomenon leads to intercarrier interference after the FFT. The output of FFT for each subcarrier contains an interfering term with interference power that is inversely proportional to the frequency spacing from all other subcarriers (Nee & Prasad, 2000). The amount of intercarrier interference for subcarriers in the middle of the OFDM spectrum is roughly twice as larger as that at the OFDM band edges because there are more interferers from interfering subcarriers on both sides. In practice, frequency-selective fading from the Doppler effect and/or mismatch and instability of the local oscillators in the transmitter and receiver cause carrier frequency offset. This effect invariably results in severe performance degradation in OFDM communications and leads to a high bit error rate. OFDM systems are more sensitive to carrier frequency offset; therefore, compensating frequency errors are very important.

## 3. Application scenarios

The major objectives for OFDM synchronization include identifying the beginning of individual OFDM symbol timing and ensuring the orthogonality of each subcarrier. Various algorithms have been proposed to estimate symbol timing and carrier frequency offset. These methods can be classified into two categories: data-aided algorithms and non-data-aided (also called blind) algorithms. By using known training sequences or pilot symbols, a data-aided algorithm can achieve high estimation accuracy and construct the structure simply. Data-aided algorithms require additional data blocks to transmit known synchronization information. Nevertheless, this method diminishes the efficiency of transmission to offer the possibility for synchronization. Non-data-aided (blind) algorithms were proposed to solve the inefficiency problem of the data-aided algorithm. Alternative techniques are based on the cyclic extension that is provided in OFDM communication systems. These techniques can achieve high spectrum efficiency but are more complicated.

In the data-aided technique, several synchronization symbols are directly inserted between the transmitted OFDM blocks; then, these pilot symbols are collected at the receiving end to extract frame timing information. However, the use of pilot symbols inevitably decreases the capacity and/or throughput of the overall system, thus making them suitable only in a startup/training mode. The data-aided technique can provide effectively synchronization with very high accuracy. Thus, it can be used to find coarse timing and frequency offset in the initial communication link. Several data-aided techniques have been proposed (Classen & Meyr, 1994, Daffara & Chouly, 1993, Kapoor et al., 1998, Luise & Reggiannini, 1996, Moose, 1994, Warner & Leung, 1993). Moreover, the SNR at the front end in the receiver is often too

low to ineffectively detect pilot symbols; thus, a blind approach is usually much more desirable. A non-data-aided technique can adjust the fine timing and frequency after the preamble signal. Some non-data-aided techniques have been proposed (Bolcskei, 2001, Daffara & Adami, 1995, Lv et al., 2005, Okada et al., 1996, Park et al., 2004, Van de Beek et al., 1997).

### 3.1 Non-data-aided method

The cyclic extension has good correlation properties because the initial  $T_{CP}$  seconds of each symbol are the same as the final seconds in OFDM communications. The cyclic prefix is used to evaluate the autocorrelation with a lag of  $T$ . When a peak is found in the correlator output, the common estimates of the symbol timing and the frequency offset can be evaluated jointly. The correlation output can be expressed as

$$x(t) = \int_0^{T_{cp}} r(t-\tau)r^*(t-\tau-T)d\tau \quad (6)$$

where  $r(t)$  is the received OFDM signal,  $x(t)$  is the correlator output,  $\tau$  denotes the timing offset. The correlator output can be utilized to estimate the carrier frequency offset when the symbol timing is found. The phase drift between  $T$  seconds is equivalent to the phase of the correlator output. Therefore, the carrier frequency offset can be estimated easily by dividing the correlator phase by  $2\pi T$ . The carrier frequency offset denotes the frequency offset normalized by the subcarrier spacing. Fig. 4 shows the block diagram of the correlator.

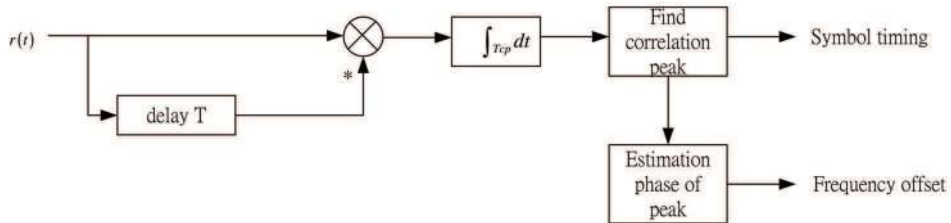


Fig. 4. Correlator using the cyclic prefix

### 3.2 Data-aided method

Although data-aided algorithms are not efficient for transmission, they have high estimation accuracy and a simple architecture which are especially important for packet transmission. The synchronization time needs to be as short as possible, and the accuracy must be as high as possible for high rate packet transmission (Nee & Prasad, 2000). Special OFDM training sequences in which the data is known to the receiver were developed to satisfy the requirement for packet transmission. The absolute received training signal can be exploited for synchronization, whereas non-data-aided algorithms that take advantage of cyclic extension only use a fraction signal of each symbol. In training sequence methods, the matched filter is used to estimate the symbol timing and carrier frequency offset. Fig. 5 shows a block diagram of a matched filter. The input signal is the known OFDM training sequence. The sampling interval is denoted as  $T$ . The elements of  $\{c_0 \ c_1 \ \dots \ c_{N-1}\}$  are the matched filter coefficients which are the complex signals of the known training sequence. The symbol timing and carrier offset can be achieved by searching for the correlation peak accumulated from matched filter outputs.

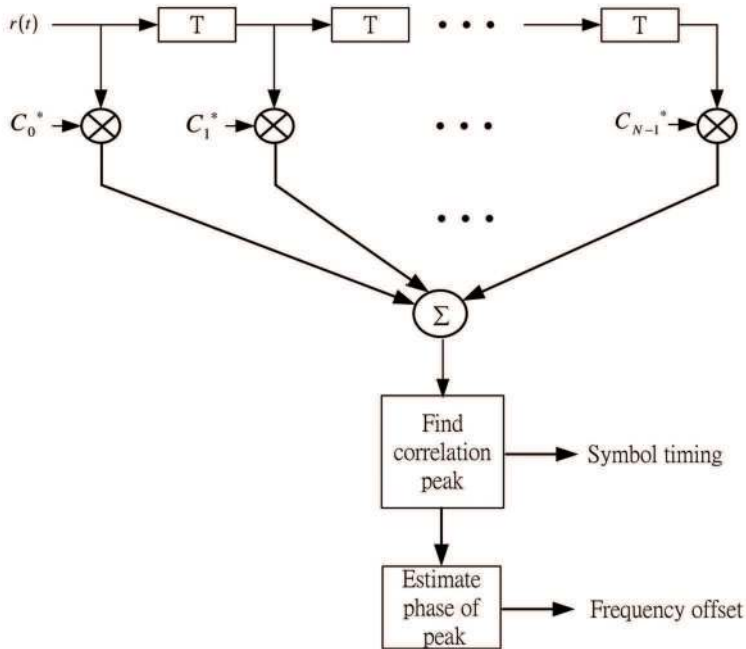


Fig. 5. Matched filter for the OFDM training sequence

### 4. Examples

#### 4.1 Example 1: Non-data-aided, CP-based, fractional/fine frequency offset

According to previous researches, very high computational complexity is required for joint estimation for timing and frequency synchronization. Moreover, one estimate suffers from performance degradation caused by estimation error of the other. Thus, an effective technique is proposed (Lin, 2003).

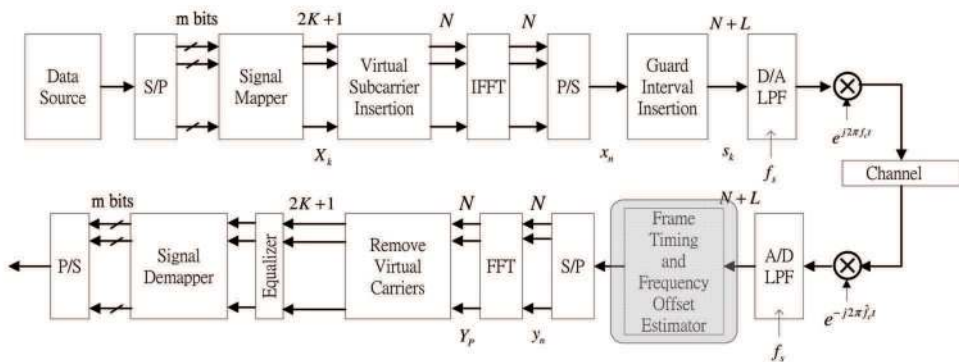


Fig. 6. The OFDM transceiver (Lin, 2003)

The proposed technique which employs a two-step method that estimates the frame timing instant and frequency offset by the maximum-likelihood (ML) estimation criterion. First, it estimates a frame timing instant such that the estimate is completely independent of the frequency offset estimation with no prior knowledge of the frequency offset; thus, a much lower estimation error of the frame timing instant is achieved by avoiding any power loss or phase ambiguity caused by frequency offset. The main reason for this arrangement is that frame timing instant estimation has to take place completely before frequency offset estimation because the latter actually requires frame timing information.

The block diagram of the OFDM system investigated here is depicted in Fig. 6. The received signal can be expressed as

$$r_k = \alpha_k s_{k-\theta} e^{j2\pi \varepsilon k/N} + n_k \tag{7}$$

where  $\theta$  is the unknown delay time;  $\alpha_k$  denotes a channel fade, which has a Rayleigh-distributed envelope and a uniformly distributed phase;  $\varepsilon$  denotes the carrier frequency offset in a subcarrier spacing; and  $1/N$  is the normalized frequency. In accordance with Jake’s model of a fading channel (Jake, 1974),  $\alpha_k$  can be expressed as a complex Gaussian random process with the autocorrelation function given as

$$E\{\alpha_{k_1} \alpha_{k_2}^*\} = J_0\left(2\pi f_D |k_1 - k_2| \frac{T_u}{N}\right) \tag{8}$$

where  $E\{\cdot\}$  denotes the statistical expectation operation;  $*$  denotes taking complex conjugation;  $J_0(\cdot)$  is the zeroth-order Bessel function of the first kind;  $f_D$  is the maximum Doppler frequency caused directly by relative motion; and  $T_u$  is the OFDM block duration, which actually corresponds to the time interval of an  $N$ -sample OFDM block. In a previous work (Van de Beek et al., 1997), the log-likelihood function for  $\theta$  and  $\varepsilon$  can be written as

$$\begin{aligned} \Lambda(\theta, \varepsilon) &= \log f(\mathbf{r}|\theta, \varepsilon) \\ &= \log \left( \prod_{k \in I} f(r_k, r_{k+N}) \prod_{k \in I \cup I'} f(r_k) \right) \\ &= \log \left( \prod_{k \in I} \frac{f(r_k, r_{k+N})}{f(r_k) f(r_{k+N})} \prod_k f(r_k) \right) \end{aligned} \tag{9}$$

where  $f(\cdot)$  denotes the probability density function;  $\mathbf{r} = [r_1 \ r_2 \ \dots \ r_{2N+L}]^T$  is the observation vector;  $I = [\theta, \theta + 1, \dots, \theta + L - 1]$ ; and  $I' = [\theta + N, \theta + N + 1, \dots, \theta + N + L - 1]$ . It must be noted that the correlations among the samples in the observation vector are exploited to estimate the unknown parameters  $\theta$  and  $\varepsilon$ , and they can be written as

$$\forall k \in I : E\{r_k, r_{k+m}^*\} = \begin{cases} E\{|r_k|^2\} = \sigma_s^2 + \sigma_n^2, & m = 0 \\ E\{r_k, r_{k+m}^*\} = \sigma_s^2 J_0(2\pi f_D T_u) e^{-j2\pi \varepsilon}, & m = N \\ 0, & \text{otherwise} \end{cases} \tag{10}$$

where  $\sigma_s^2 = E[|s_k|^2]$  is the average signal power and  $\sigma_n^2 = E[|n_k|^2]$  is the average noise power.

Because the product  $\prod_k f(r_k)$  in (9) is independent of  $\theta$  and  $\varepsilon$ , it can be dropped when maximizing  $\Lambda(\theta, \varepsilon)$ . Under the assumption that  $\mathbf{r}$  is a jointly Gaussian vector and after some manipulations reported in the reference Appendix (Lin, 2003), (9) can be rewritten as

$$\begin{aligned} \Lambda(\theta, \varepsilon) &= c_1 + c_2 \left[ \sum_{k=\theta}^{\theta+L-1} \operatorname{Re}\{r_k r_{k+N}^* e^{-j2\pi\varepsilon}\} - \frac{\rho}{2} \sum_{k=\theta}^{\theta+L-1} (|r_k|^2 + |r_{k+N}|^2) \right] \\ &= c_1 + c_2 \left[ \operatorname{Re}\{\lambda_1(\theta)\} \cos(2\pi\varepsilon) - \operatorname{Im}\{\lambda_1(\theta)\} \sin(2\pi\varepsilon) - \rho\lambda_2(\theta) \right] \end{aligned} \quad (11)$$

where

$$\begin{aligned} \rho &= \frac{E\{r_k r_{k+N}^*\}}{\sqrt{E\{|r_k|^2\} E\{|r_{k+N}|^2\}}} = \frac{\sigma_s^2 J_0(2\pi f_D T_u)}{\sigma_s^2 + \sigma_n^2} \\ c_1 &= - \sum_{k=\theta}^{\theta+L-1} \log(1 - \rho^2) \\ c_2 &= \frac{2\rho}{(1 - \rho^2)(\sigma_s^2 + \sigma_n^2)} \\ \lambda_1(\theta) &= \sum_{k=\theta}^{\theta+L-1} r_k r_{k+N}^* \\ \lambda_2(\theta) &= \frac{1}{2} \sum_{k=\theta}^{\theta+L-1} \{|r_k|^2 + |r_{k+N}|^2\} \end{aligned}$$

In the above equation, it is assumed that the random frequency modulation caused by a time-varying channel fade and the phase noise of the local oscillator are negligible; thus,  $\{r_k r_{k+N}^*\}$  has almost the same phase within the range  $k \in [\theta, \theta + L - 1]$ ; therefore,  $\{r_k r_{k+N}^*\}$  can be coherently summed up in the term  $\lambda_1(\theta)$ . If the partial derivative of  $\Lambda(\theta, \varepsilon)$  is taken with respect to  $\varepsilon$ , one can obtain the following equation:

$$\frac{\partial}{\partial \varepsilon} \Lambda(\theta, \varepsilon) = -2\pi c_2 \left[ \operatorname{Re}\{\lambda_1(\theta)\} \sin(2\pi\varepsilon) + \operatorname{Im}\{\lambda_1(\theta)\} \cos(2\pi\varepsilon) \right] \quad (12)$$

To obtain the value of  $\hat{\varepsilon}$  that maximizes  $\Lambda(\theta, \varepsilon)$ , the above partial derivative is set to zero and equality stands only when

$$\frac{\operatorname{Re}\{\lambda_1(\theta)\}}{\cos(2\pi\varepsilon)} = \frac{\operatorname{Im}\{\lambda_1(\theta)\}}{-\sin(2\pi\varepsilon)} = \frac{1}{c_3} \quad (13)$$

where  $c_3$  is set as a constant  $1/L$  for simplicity. As a result, the carrier frequency offset estimate can be expressed as

$$\hat{\varepsilon} = -\frac{1}{2\pi} \tan^{-1} \left( \frac{\operatorname{Im}\{\lambda_1(\theta)\}}{\operatorname{Re}\{\lambda_1(\theta)\}} \right) \quad (14)$$



The carrier frequency offset estimator derived above actually requires accurate frame timing information to effectively resolve the carrier frequency offset by taking advantage of a complete cyclic prefix. As a result, accurate frame timing estimation has to be performed before a carrier frequency offset is estimated.

To develop a frame timing estimation scheme without prior knowledge of frequency offset, the log-likelihood function in (11) can be approximated as follows:

$$\begin{aligned} \Lambda(\theta, \varepsilon) &\approx c_1 + c_2 \left[ c_3 \operatorname{Re}\{\lambda_1(\theta)\} \cdot \operatorname{Re}\{\lambda_1(\theta)\} + c_3 \operatorname{Im}\{\lambda_1(\theta)\} \cdot \operatorname{Im}\{\lambda_1(\theta)\} - \rho \lambda_2(\theta) \right] \\ &= c_1 + c_2 \left[ c_3 \left( \operatorname{Re}^2\{\lambda_1(\theta)\} + \operatorname{Im}^2\{\lambda_1(\theta)\} \right) - \rho \lambda_2(\theta) \right] \\ &= c_1 + c_2 \left[ c_3 |\lambda_1(\theta)|^2 - \rho \lambda_2(\theta) \right] \end{aligned} \tag{15}$$

Thus, one can obtain a frame timing estimator independent of frequency offset estimation. The proposed technique provides a more practical estimate of the frame timing instant because frame timing estimation is very often performed before frequency offset is estimated or dealt with. As a result, the proposed estimator of the frame timing instant and frequency offset can be expressed as

$$\begin{cases} \text{Step 1: } \hat{\theta}_p = \arg \max_{\theta} \left\{ c_3 |\lambda_1(\theta)|^2 - \rho \lambda_2(\theta) \right\} \\ \text{Step 2: } \hat{\varepsilon}_p = -\frac{1}{2\pi} \tan^{-1} \left( \frac{\operatorname{Im}\{\lambda_1(\hat{\theta}_p)\}}{\operatorname{Re}\{\lambda_1(\hat{\theta}_p)\}} \right) \end{cases} \tag{16}$$

Its structure is depicted in detail in Fig. 7. The proposed frame timing estimator inherently exploits the highest signal level by disregarding any phase ambiguity caused by residual error in frequency offset estimation. Therefore, the proposed technique performs frame timing estimation in a manner independent of frequency offset estimation; then, frequency offset estimation can be properly achieved in the next step by effectively taking advantage of accurate timing information.

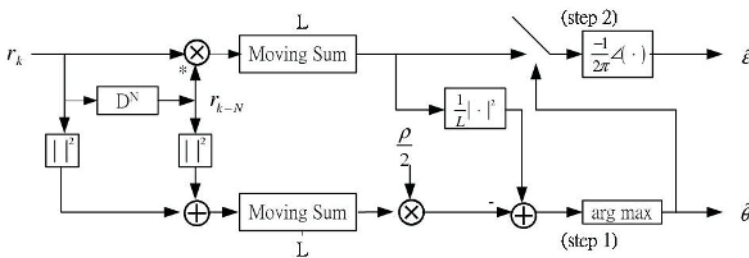


Fig. 7. The estimator (Lin, 2003)

Because the effect of fast channel fading is considered here, the proposed technique has to account for a maximum Doppler frequency  $f_D$  on the same order of  $1/T_u$ . Therefore, the proposed estimator of the frame timing instant is often dominated by its first term because the correlation coefficient term  $\rho$  in (16) approaches zero in such an environment. As a result, estimating of the frame timing instant can be simplified as follows to reduce the hardware complexity:

$$\hat{\theta}'_p = \arg \max_{\theta} \left\{ \left| \lambda_1(\theta) \right|^2 \right\} \tag{17}$$

In addition, several techniques for combining multiple frames have also been investigated (Lin, 2003) to increase the robustness of the proposed technique under low SNR conditions. Other simulation experiments show that the proposed techniques can effectively achieve lower estimation errors in frame timing and frequency offset estimation.

**4.2 Example 2: Data-aided, preamble, integral/coarse frequency offset**

Previous works often employ signal-estimation techniques on a time-indexed basis in the time direction. However, very few previous works have dealt with frequency-offset problems by applying a detection technique on a subcarrier-indexed basis in the frequency direction. An effective technique for frequency acquisition based on maximum-likelihood detection for mobile OFDM is proposed. The proposed technique employs a frequency-acquisition stage and a tracking stage. We mainly focus on frequency acquisition because tracking has been investigated (Lin, 2004, 2006b, 2007). By exploiting differential coherent detection of a single synchronization sequence, where a pseudonoise (PN) sequence is used as a synchronization sequence, we can prove that data-aided frequency acquisition with frequency-directional PN matched filters (MFs) reduces the probabilities of false alarm and miss on a channel with a sufficiently wide coherence bandwidth. Strict statistical analyses have been performed to verify the improvements achieved. Furthermore, the proposed technique can operate well over a channel with severe frequency-selective fading by exploiting subcarrier-level differential operation and subsequent coherent PN cross-correlation.

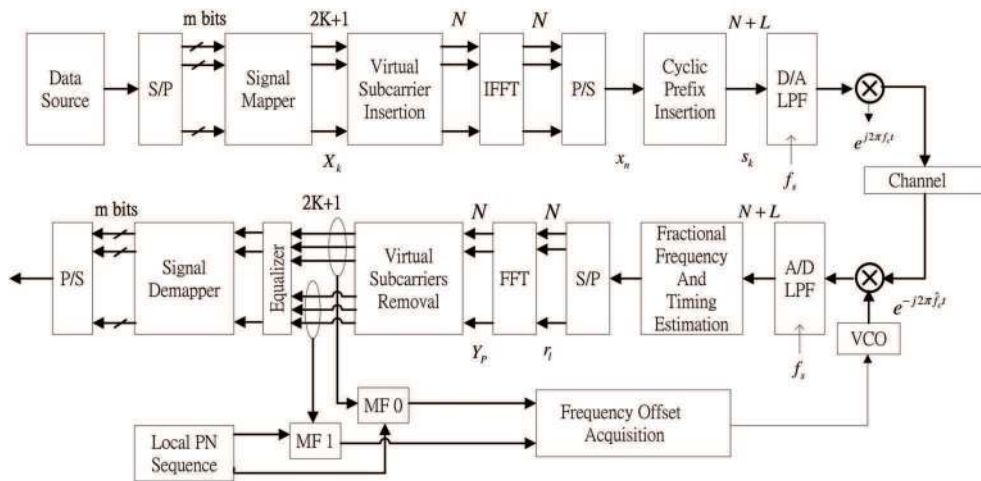


Fig. 8. The OFDM transceiver (Lin, 2006a)

In the investigated OFDM system, a PN sequence with a period  $N_p$  (say,  $N_p < K$ ) is successively arranged to form an OFDM preamble block. The complex representation of the received baseband-equivalent signal can, thus, be written as

$$r_l = \frac{1}{\sqrt{N}} \sum_{k=-K}^K c_{|k|_{N_p}} \exp\left(j2\pi \frac{kl}{N}\right) \exp\left(j2\pi(d+\varepsilon)\frac{l}{N}\right) + n_l^m, \quad l=0,1,\dots,N-1 \quad (18)$$

where  $l$  denotes the time index, the term  $\exp(j2\pi(d+\varepsilon)(l/N))$  represents the effect of the CFO that is mainly caused by instability or mismatch that occurs with the local oscillator at the front-end down-conversion process,  $d$  and  $\varepsilon$  are the integral and fractional parts of the CFO, respectively, which are normalized by the subcarrier spacing (i.e., frequency separation between any two adjacent subcarriers),  $c_{|k|_{N_p}}$  is the  $|k|_{N_p}$ th chip value of the PN code transmitted via the  $k$ th subchannel, whose normalized subcarrier frequency is  $(k/N)$ ,  $|k|_{N_p}$  denotes the  $k$  modulus  $N_p$ , and  $n_l^m$  is complex white Gaussian noise. With the FFT demodulation, the  $p$ th subchannel output can be expressed as

$$\begin{aligned} Y_p &= \frac{1}{\sqrt{N}} \sum_{l=0}^{N-1} \exp\left(-j2\pi \frac{pl}{N}\right) \cdot r_l \\ &= \sum_{k=-K}^K c_{|k|_{N_p}} g(k+d-p+\varepsilon) \cdot \exp\left(j\pi \frac{N-1}{N}(k+d-p+\varepsilon)\right) + n_p^m, \quad p=-N/2, \dots, N/2-1 \end{aligned} \quad (19)$$

where

$$g(v) = \frac{\sin(\pi v)}{N \sin(\pi v/N)}$$

and  $n_p^m$  has a noise term. If the demodulation outputs  $\{Y_p, p=0,1,\dots,N_p-1; N_p < K\}$  are cross-correlated with a locally generated PN sequence with a phase delay  $\hat{d}$  using PN MF, then the output of the PN MF can be obtained.

$$Z_0 = \frac{\sqrt{N_p}}{\sigma_0} g(d-\hat{d}+\varepsilon) \exp\left(j\pi \frac{N-1}{N}(d-\hat{d}+\varepsilon)\right) + n_0 \quad (20)$$

The detailed derivation has been shown elsewhere (Lin, 2006a). As a result, coarse frequency offset can be detected through subcarrier acquisition. The detection procedure is equivalent to testing the following two hypotheses:

$$\begin{cases} f_{\|Z_0\|^2}(\eta|A_1, H_1) \sim \chi^2 \\ A_1 = g_1(\varepsilon) = \frac{\sin(\pi\varepsilon)}{N \sin(\pi\varepsilon/N)} = g(\varepsilon), \quad H_1: d = \hat{d}, \\ f_{\|Z_0\|^2}(\eta|A_0, H_0) \sim \chi^2 \\ A_0 = g_0(\varepsilon) = g(d'+\varepsilon) = \frac{\sin(\pi(d'+\varepsilon))}{N \sin(\pi(d'+\varepsilon)/N)} \Big|_{d'=d-\hat{d} \neq 0}, \quad H_0: d \neq \hat{d} \end{cases} \quad (21)$$

where  $H_1$  and  $H_0$  denote the two hypothesis that the local PN sequence has been aligned (i.e.,  $d = \hat{d}$ ) and has not been aligned in-phase (i.e.,  $d \neq \hat{d}$ ), respectively, with respect to the post-FFT-demodulation PN sequence.

The previous derivations show that the major difficulty with the ordinary likelihood functions results from the very complicated probability density functions of the derived

random variable,  $A_0 = g_0(\varepsilon)$  and  $A_1 = g_1(\varepsilon)$ . Therefore, the two derived random variables  $A_0$  and  $A_1$  are first set to be constant for the worst cases, and thus, the (fixed) noncentrality parameters can be exploited in the likelihood functions to simplify the detection procedure. The probabilities of false alarm and miss for noncoherent detection can be written as

$$\begin{aligned} P_{fa}^{nc}(t_{nc}) &= P(S > t_{nc} | H_0) \\ &\leq \int_{t_{nc}}^{\infty} f_S(s | H_0, \max_{\varepsilon} g_0(\varepsilon)) ds \\ &= Q_1(\sqrt{\lambda_{nc,0}}, t_{nc}) \end{aligned} \quad (22)$$

$$\begin{aligned} P_{ms}^{nc}(t_{nc}) &= P(S \leq t_{nc} | H_1) \\ &\leq 1 - \int_{t_{nc}}^{\infty} f_S(s | H_1, \min_{\varepsilon} g_1(\varepsilon)) ds \\ &= 1 - Q_1(\sqrt{\lambda_{nc,1}}, t_{nc}) \end{aligned} \quad (23)$$

where

$$\begin{aligned} \lambda_{nc,0} &= \max_{\substack{|\varepsilon| \leq 0.5 \\ d \neq \hat{d}}} \left| \frac{\sin(\pi(d - \hat{d} + \varepsilon))}{N \sin(\pi(d - \hat{d} + \varepsilon)/N)} \frac{\sqrt{N_p}}{\sigma_0} \right|^2 \doteq 2g^2(1.5)N_p \cdot \overline{SNR} \\ \lambda_{nc,1} &= \max_{\substack{|\varepsilon| \leq 0.5 \\ d = \hat{d}}} \left| g(d - \hat{d} + \varepsilon) \frac{\sqrt{N_p}}{\sigma_0} \right|^2 = 2g^2(0.5)N_p \cdot \overline{SNR} \end{aligned}$$

and

$$Q_{\mu/2}(a, b) = \int_b^{\infty} \frac{1}{2} \left( \frac{x}{a^2} \right)^{(\mu-2)/4} \cdot \exp\left(-\frac{x+a^2}{2}\right) I_{\frac{\mu-1}{2}}(\sqrt{a^2 x}) dx$$

is the generalized Marcum Q-function, which is defined as the complementary cumulative density function of a noncentral  $\chi^2$  random variable with  $\mu$  degrees of freedom and noncentrality parameter  $a^2$ , and where  $t_{nc}$  is a design parameter representing the decision threshold of the derived noncoherent detection.

The above noncoherent detector can be further improved by a differentially coherent detection technique that consists of coherent accumulation of cross-correlations subchannel-by-subchannel by means of PN MFs. The detailed derivation has been provided elsewhere (Lin, 2006a). As a result, the probability of false alarm and miss for the proposed differentially coherent subcarrier-acquisition technique is given by

$$P_{fa}^{dc} = P(\gamma_a - \gamma_b > t_{dc} | H_0) = \int_0^{\infty} f_{\gamma_b}(s | H_0) \int_{s+t_{dc}}^{\infty} f_{\gamma_a}(\eta | H_0) d\eta ds = \int_0^{\infty} \frac{1}{2} e^{-s/2} Q_1(\sqrt{\lambda_{dc,0}}, s + t_{dc}) ds \quad (24)$$

$$P_{fa}^{dc} = P(\gamma_a - \gamma_b \leq t_{dc} | H_1) = 1 - \int_0^{\infty} \frac{1}{2} e^{-s/2} Q_1(\sqrt{\lambda_{dc,1}}, s + t_{dc}) ds \quad (25)$$

where

$$\lambda_{dc,0} = \Lambda^2 \left|_{\substack{H_0 \\ d \neq \hat{d}}} = 4g^2(1.5)N_p \overline{SNR}$$

$$\lambda_{dc,1} = \Lambda^2 \left|_{\substack{H_1 \\ d = \hat{d}}} = 4g^2(0.5)N_p \overline{SNR}$$

and  $t_{dc}$  is a design parameter denoting the decision threshold when the above differentially coherent detection is used.

It can be easily seen from simulation results (Lin, 2006a) that no matter what values of the decision threshold are chosen, the proposed techniques can achieve sufficiently low probabilities of false alarm and miss and that differentially coherent detection can achieve lower probabilities than its noncoherent counterpart. The main reason for this difference is that differentially coherent detection primarily tests two more distantly separated distributions than does the noncoherent detection.

Although the previous derivations were conducted only on an AWGN channel, similar results and conclusions hold for a flat-fading channel or in an environment whose coherence bandwidth is wide enough to accommodate several subchannels. The relative contexts are shown completely in the reference paper (Lin, 2006a).

## 5. Synchronization in LTE/LTE-A systems

### 5.1 Introduction

Requirement of transmission data rate grows up rapidly as time flies. The Long Term Evolution (LTE) specification proposed by 3rd Generation Partnership Project (3GPP) has a significant influence on recent wireless communications. LTE communication systems are expected to achieve a data rate of 100 Mb/s on downlink and 50 Mb/s on uplink transmissions; it can also provide flexible bandwidths of 1.4, 2.5, 5, 10, 15 and 20 MHz. An LTE communication is based on the OFDM techniques and adopts single-carrier frequency-division multiple access (SC-FDMA) on uplink transmission and OFDMA on downlink transmission. It is clear that LTE can provide a high data rate, robust performance over multipath fading channels and high spectral efficiency. However, an LTE system has a major drawback: it is sensitive to frequency error as OFDM systems. Timing and frequency synchronization is a key component for initial synchronization of an LTE system. For a link initiative, a mobile station has to search for a base-station by means of synchronization sequences, which are broadcasted in all directions in which the station provides coverage. This search is called *cell search* in cellular systems. In the cell search, a sector search must be performed at first. The following tasks comprise the sector search: coarse timing alignment, fine timing synchronization, fine frequency offset compensation, coarse frequency offset detection, and sector identification.

### 5.2 LTE frame structure

An LTE supports 504 different cell identifications. To avoid the high complexity of a cell search procedure, these cell identifications are categorized into 168 cell-identification groups,  $N_{ID}^{(1)}$ ; additionally, each cell-identification group contains three identities,  $N_{ID}^{(2)}$ . Therefore, cell identification (ID) can be stated as  $N_{ID}^{cell} = 3N_{ID}^{(1)} + N_{ID}^{(2)}$ . Initially, the sector of the received signal has to be identified. Then, the cell that can provide service must be identified. After the above procedure is completed, communication can begin. An LTE supports two

synchronization signals for the cell search procedure. One is the primary synchronization signal (P-SCH), and the other is the secondary synchronization signal (S-SCH). P-SCH and S-SCH are inserted into the last two OFDM symbols in the first slot of the sub-frame zero and sub-frame five, where the frame structure is shown in Fig. 9. The P-SCH signal is transmitted twice in each 10-ms frame. It can provide frame timing synchronization with a tolerance of 5 ms. The main goal of the P-SCH is to conduct timing synchronization, coarse frequency-offset detection and sector identification. Each frame has a pair of S-SCH signals that can be chosen from the 168 different cell identifications. Therefore, the S-SCH signal is used to determine the cell ID.

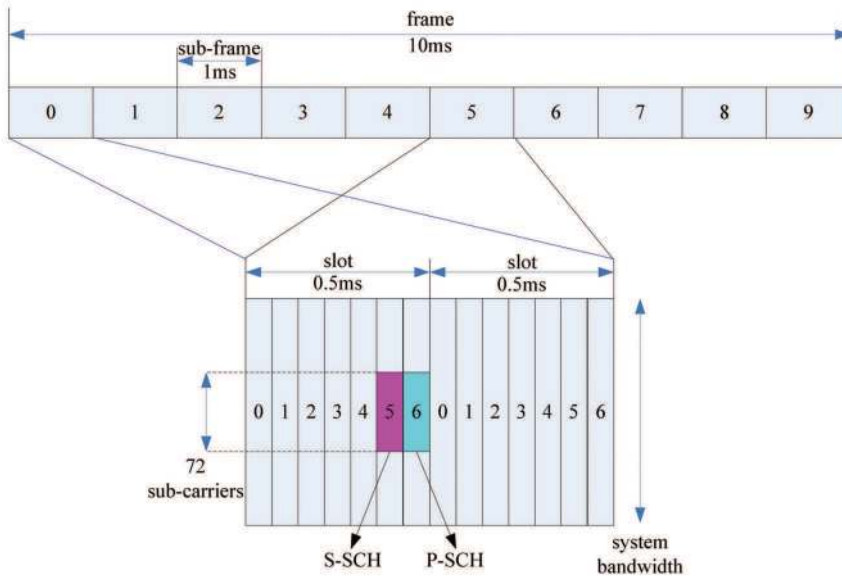


Fig. 9. LTE frame structure

The frame structure of the LTE system is depicted in Fig. 9, and the length of each frame is 10 ms. Each frame is divided into ten 1-ms sub-frames. Each sub-frame contains two slots with lengths 0.5 ms. Additionally, each slot consists of seven symbols, and each symbol contains 2048 samples. The zeroth and fifth sub-frame convey P-SCH and S-SCH signals. According to the LTE specification, the CP length is 160 samples in the first symbol of a slot and 144 samples in the other 6 symbols of the slot. When the occupied bandwidth is 20 MHz, the system parameters are as follows: the sampling rate is 30.72 MHz, the FFT size is 2048, and the subcarrier spacing is 15 KHz. The synchronization signals occupy only the central 72 sub-carriers of the 2048 sub-carriers. Both boundaries of the band conveying the synchronization signals accommodate 5 null subcarriers. Therefore, the synchronization signals only adopt 62 subcarriers.

### 5.3 P-SCH signal

The number of physical-layer cell identifications is very large. To avoid high complexity in the cell search, the cell identifications are partitioned into three sets, physical-layer cell-identification group  $N_{ID}^{(2)}$  or sector. The P-SCH signal is composed of three Zadoff-Chu (ZC)

sequences with lengths of 62 in the frequency domain. Each sequence represents a sector identification. The ZC sequences employed in the LTE (3GPP LTE, 2005) are written as

$$d_u(n) = \begin{cases} e^{-j \frac{\pi u n(n+1)}{63}}, & n = 0, 1, \dots, 30 \\ e^{-j \frac{\pi u (n+1)(n+2)}{63}}, & n = 31, 32, \dots, 61. \end{cases} \quad (26)$$

$N_{ID}^{(2)}$	Root index $u$
0	25
1	29
2	34

Table 1. Root index  $u$  of sector identification (3GPP LTE, 2005)

where  $u$  is the root index for which values are set to 25, 29, and 34, which correspond to  $N_{ID}^{(2)} = 0, 1$  or 2, respectively. A ZC sequence is a chirp-like sequence and is symmetric both in the time domain and frequency domain. The sequence has good correlation properties. Therefore, the P-SCH signal employing the ZC sequence is utilized to help coarse timing synchronization and frequency-offset detection.

#### 5.4 Cell search method

Research regarding sector search in LTE systems has been studied extensively (Chen et al., 2009, Manolakis et al., 2009, Tsai et al., 2007). Three methods were studied previously (Tsai et al., 2007). They mainly take advantage of auto-correlation, cross-correlation and hybrid detection. The first method adopts auto-correlation to search for P-SCH location by taking advantage of the repetitions of P-SCH sequences. Coarse frequency-offset acquisition depends on the output of the auto-correlator. Its main advantage is low complexity, but the timing detection is inevitably distorted on signals with low SNR. The second method employs cross-correlation between the received signal and the locally-generated P-SCH to detect timing and frequency offset. Additionally, the cross-correlation can be divided into several segments to counter any effect caused by a high frequency offset. The method has a trustworthy timing detection, but its complexity is higher than auto-correlation detection. Hybrid detection combines advantages of auto-correlation and cross-correlation. Its complexity is less than that employing cross-correlation detection. The auto-correlation detection obtains coarse timing and frequency offset, and compensates for the frequency error. Then, the accurate timing can be obtained by exploiting cross-correlation. A previous study (Manolakis et al., 2009) used maximum likelihood (ML) criterion to estimate the fractional frequency offset and the OFDM symbol timing; its performance is improved by averaging 8 OFDM symbols. Next, cross-correlation between the three P-SCH sequences and the received signal is obtained; and the sector ID can be determined by selecting the highest cross-correlation according to the orthogonality among the used Zadoff-Chu sequences.

#### 5.5 Carrier aggregation

Carrier aggregation is one of the most important technologies in the new LTE-Advanced standards. This technique will also play a significant role for 4G communication systems. By

using carrier aggregation, a peak data rate up to 1 Gb/s is possible in future 4G mobile communications. Because of the flexibility of effective transmission, the user can exploit numerous carriers at the same time. In addition, these carriers may lie in the same or different band and may have different bandwidths. Carrier aggregation provides diverse combinations and flexible spectrum usability and has attracted attention. Carrier aggregation techniques can be classified into two categories: continuous and discontinuous as shown in Fig. 10. These two categories can be subdivided into three types: intraband contiguous, intraband discontinuous and interband. A diagram describes their difference in Fig. 11.

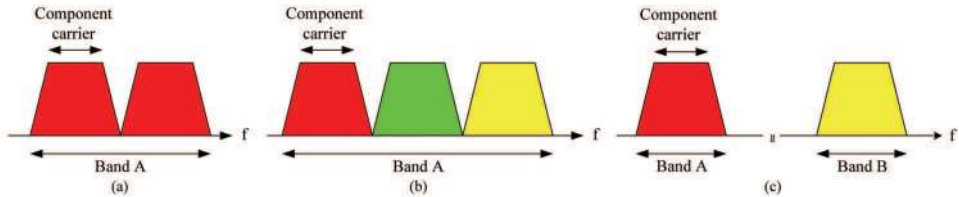


Fig. 10. Carrier aggregation types: (a) intraband contiguous; (b) intraband discontinuous; (c) interband (Iwamura et al., 2010)

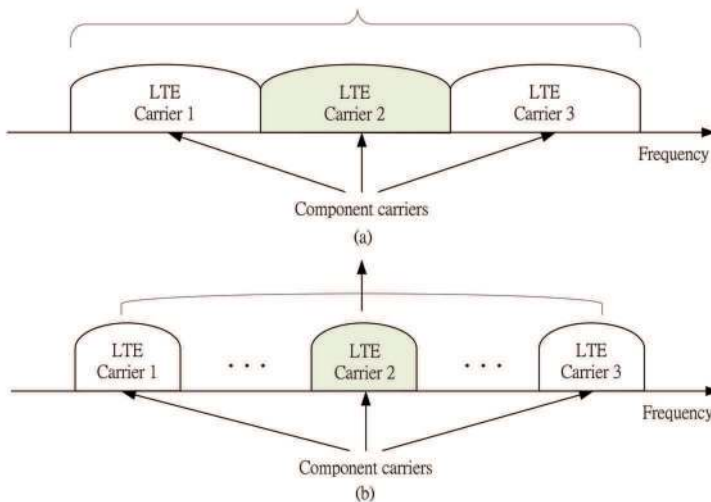


Fig. 11. Carrier aggregation categories: (a) continuous; (b) discontinuous (Yuan et al., 2010)

## 6. Summary

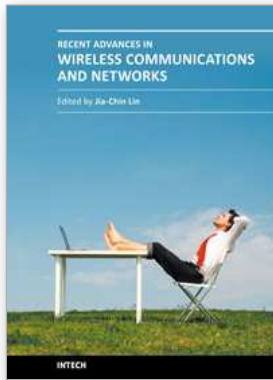
In this chapter, the authors intend to introduce the OFDM communication systems and take care of the main issue, frequency offset, can lead to severe performance degradation. Two classifications of synchronization techniques are introduced. Several novel techniques have been thoroughly discussed in great detail in this chapter. LTE/LTE-A systems have been chosen as candidates for 4G mobile communication. The concept of LTE-LTE-A systems is mentioned in the end of this chapter.



## 7. References

- 3GPP LTE (2005). TS 36.211 V8.3.0: Technical Specification Group Radio Access Network; Evolved Universal Terrestrial Radio Access (E-UTRA); Physical Channels and Modulation (Release 8)
- Bolskei, H. (2001). Blind estimation of symbol timing and carrier frequency offset in wireless OFDM systems, *IEEE Transactions on Communications*, Vol.49, No.6, (June 2001), pp.988-999
- Chen, Y., Wen, X., Zheng, W. & Lin, X. (2009). Symbol timing estimation and sector detection algorithm based on LTE TDD system, *Proceedings of IEEE Network Infrastructure and Digital Content Conference, 2009 (IC-NIDC 2009)*, Beijing, China, pp.828-832.
- Classen, F. & Meyr, H. (1994). Frequency synchronization algorithms for OFDM systems suitable for communication over frequency selective fading channels, *Proceedings of IEEE Vehicular Technology Conference, 1994 (VTC'94)*, Stockholm, Sweden, pp. 1655-1659
- Daffara, F. & Chouly, A. (1993). Maximum likelihood frequency detectors for orthogonal multicarrier systems, *Proceedings of IEEE Communications Conference, 1993 (ICC'93)*, Geneva, Switzerland, pp. 766-771
- Daffara, F. & Adami, O. (1995). A new frequency detector for orthogonal multicarrier transmission techniques, *Proceedings of IEEE Vehicular Technology Conference, 1995 (VTC'95)*, Chicago, USA, pp. 804-809
- Dahlman, E., Parkvall, S., Skold, J. & Beming, P. (2007) *3G Evolution HSPA and LTE for Mobile Broadband*, Academic Press
- Iwamura, M., Etemad, K., Fong M.-H., Nory, R. & Love, R. (2010) Carrier aggregation framework in 3GPP LTE-advanced [WiMAX/LTE update], *IEEE Communications Magazine*, Vol.48, No.8, (August 2010), pp.66-67
- Jakes, W. C. & Cox, D. C. (1994). *Microwave Mobile Communications*. Wiley-IEEE Press
- Kapoor, S., Marchok, D. J. & Huang, Y.-F. (1998). Pilot assisted synchronization for wireless OFDM systems over fast time varying fading channels, *Proceedings of IEEE Vehicular Technology Conference, 1998 (VTC'98)*, Ottawa, Canada, pp. 2077-2080
- Lin, J.-C. (2002a). Noncoherent sequential PN code acquisition using sliding correlation for chip-asynchronous DS/SS, *IEEE Transactions on Communications*, Vol.50, No.4, (April 2002), pp.664-676
- Lin, J.-C. (2002b). Differentially coherent PN code acquisition with full-period correlation in chip-asynchronous DS/SS receivers, *IEEE Transactions on Communications*, Vol.50, No.5, (May 2002), pp.698-702
- Lin, J.-C. (2002c). Differentially coherent PN code acquisition based on a matched filter for chip-asynchronous DS/SS communications, *IEEE Transactions on Vehicular Technology*, Vol.51, No.6, (November 2002), pp.1596-1599
- Lin, J.-C. (2003). Maximum-likelihood frame timing instant and frequency offset estimation for OFDM communication over a fast Rayleigh-fading channel, *IEEE Transactions on Vehicular Technology*, Vol.52, No.4, (July 2003), pp.1049-1062
- Lin, J.-C. (2004). Frequency offset estimation by differentially coherent frequency error characterization for OFDM wireless communications, *Proceedings of IEEE Communications Conference, 2004 (ICC'04)*, Paris, France, pp. 2387-2391.
- Lin, J.-C. (2005). Frequency offset acquisition based on subcarrier differential detection for OFDM communications on doubly-selective fading channel, *Proceedings of IEEE Communications Conference, 2005 (ICC'05)*, Seoul, Korea, pp. 1952-1956.

- Lin, J.-C. (2006a). Coarse frequency-offset acquisition via subcarrier differential detection for OFDM communications, *IEEE Transactions on Communications*, Vol.54, No.8, (August 2006), pp.1415-1426
- Lin, J.-C. (2006b). Frequency offset estimation technique based on error characterization for OFDM communications on time-varying multipath fading channels, *Proceedings of IEEE Communications Conference, 2006 (ICC'06)*, Istanbul, Turkey, pp.2911-2916.
- Lin, J.-C. (2007). A frequency offset estimation technique based on frequency error characterization for OFDM communications on multipath fading channels, *IEEE Transactions on Vehicular Technology*, Vol.56, No.3, (May 2007), pp.1209-1222
- Luise, M. & Reggiannini, R. (1996). Carrier frequency acquisition and tracking for OFDM systems, *IEEE Transactions on Communications*, Vol.44, No.11, (November 1996), pp.1590-1598
- Lv, T., Li, H. & Chen, J. (2005) Joint estimation of symbol timing and carrier frequency offset of OFDM signals over fast time-varying multipath channels, *IEEE Transaction on Signal Processing*, Vol.53, No.12, (December 2005), pp.4526-4535
- Manolakis, K., Gutierrez Estevez, D. M., Jungnickel, J., Xu, W. & Drewes, C. (2009) A closed concept for synchronization and cell Search in 3GPP LTE systems, *Proceedings of IEEE Wireless Communications and Networking Conference, 2009 (WCNC 2009)*, Budapest, Hungary, pp. 1-6.
- Moose, P. H. (1994). A technique for orthogonal frequency division multiplexing frequency offset correction, *IEEE Transactions on Communications*, Vol.42, No.10, (October 1994), pp.2908-2914
- Nee, V. R. & Prasad, R., (2000). *OFDM for Wireless Multimedia Communications*, Artech House
- Okada, M., Hara, S., Komaki, S. & Morinaga, N. (1996). Optimum synchronization of orthogonal multi-carrier modulated signals, *Proceedings of IEEE Personal, Indoor and Mobile Radio Communications Conference, 1996 (PIMRC'96)*, Taipei, Taiwan, pp. 863-867
- Park, B., Ko, E., Cheon, H., Kang, C. & Hong, D. (2001). A Blind OFDM synchronization algorithm based on cyclic correlation, *IEEE Signal Processing Letters*, Vol.11, No.2, (February 2004), pp.83-85.
- Popovic, B. M. (1992). Generalized chirp-like polyphase sequences with optimum correlation properties, *IEEE Transactions on Information Theory*, Vol.38, No.4, (July 1992), pp.1406-1409
- Van de Beek, J.-J., Sandell, M. & Borjesson, P. O. (1997). ML estimation of time and frequency offset in OFDM systems, *IEEE Transaction on Signal Processing*, Vol.45, No.7, (July 1997), pp. 1800-1805
- Tsai, Y., Zhang, G., Grieco, D. & Ozluturk, F. (2007). Cell search in 3GPP Long Term Evolution systems, *IEEE Vehicular Technology Magazine*, Vol.2, No.2, (June 2007), pp.23-29
- Warner, W. D. & Leung, C. (1993). OFDM/FM frame synchronization for mobile radio data communications, *IEEE Transactions on Vehicular Technology*, Vol.42, No.3, (August 1993), pp.302-313
- Yuan, G., Zhang, X., Wang, W. & Yang, Y. (2010). Carrier Aggregation for LTE-advanced mobile communication systems, *IEEE Transaction on Communication Magazine*, Vol.48, No.2, (February 2010), pp.88-93



## **Recent Advances in Wireless Communications and Networks**

Edited by Prof. Jia-Chin Lin

ISBN 978-953-307-274-6

Hard cover, 454 pages

**Publisher** InTech

**Published online** 23, August, 2011

**Published in print edition** August, 2011

This book focuses on the current hottest issues from the lowest layers to the upper layers of wireless communication networks and provides “real-time” research progress on these issues. The authors have made every effort to systematically organize the information on these topics to make it easily accessible to readers of any level. This book also maintains the balance between current research results and their theoretical support. In this book, a variety of novel techniques in wireless communications and networks are investigated. The authors attempt to present these topics in detail. Insightful and reader-friendly descriptions are presented to nourish readers of any level, from practicing and knowledgeable communication engineers to beginning or professional researchers. All interested readers can easily find noteworthy materials in much greater detail than in previous publications and in the references cited in these chapters.

### **How to reference**

In order to correctly reference this scholarly work, feel free to copy and paste the following:

Yu-Ting Sun and Jia-Chin Lin (2011). Synchronization for OFDM-Based Systems, Recent Advances in Wireless Communications and Networks, Prof. Jia-Chin Lin (Ed.), ISBN: 978-953-307-274-6, InTech, Available from: <http://www.intechopen.com/books/recent-advances-in-wireless-communications-and-networks/synchronization-for-ofdm-based-systems>

# **INTECH**

open science | open minds

### **InTech Europe**

University Campus STeP Ri  
Slavka Krautzeka 83/A  
51000 Rijeka, Croatia  
Phone: +385 (51) 770 447  
Fax: +385 (51) 686 166  
[www.intechopen.com](http://www.intechopen.com)

### **InTech China**

Unit 405, Office Block, Hotel Equatorial Shanghai  
No.65, Yan An Road (West), Shanghai, 200040, China  
中国上海市延安西路65号上海国际贵都大饭店办公楼405单元  
Phone: +86-21-62489820  
Fax: +86-21-62489821

© 2011 The Author(s). Licensee IntechOpen. This chapter is distributed under the terms of the [Creative Commons Attribution-NonCommercial-ShareAlike-3.0 License](#), which permits use, distribution and reproduction for non-commercial purposes, provided the original is properly cited and derivative works building on this content are distributed under the same license.